Dynamics of camphor sulphonic acid: A quasielastic neutron scattering study

ARTICLE *in* CHEMICAL PHYSICS · MARCH 2002

Impact Factor: 1.65 · DOI: 10.1016/S0301-0104(02)00313-0

4 AUTHORS, INCLUDING:

David Djurado
French National Centre for Scientific R…
137 PUBLICATIONS **1,762** CITATIONS
SEE PROFILE

Jérôme Combet
University of Strasbourg
58 PUBLICATIONS **358** CITATIONS
SEE PROFILE

ELSEVIER

Chemical Physics 277 (2002) 211–224

Chemical Physics

www.elsevier.com/locate/chemphys

Dynamics of camphor sulphonic acid: a quasielastic neutron scattering study

M. Bée[a,b,1], D. Djurado[a,*], J. Combet[c], M.A. Gonzalez[b]

[a] *Laboratoire de Spectrométrie Physique, Université Joseph Fourier Grenoble-I, B.P. 87, 38402 Saint-Martin d'Hères Cedex, France*
[b] *Institut Laue-Langevin, 6 rue Jules Horowitz, B.P. 156, 38042 Grenoble Cedex, France*
[c] *Institut Charles Sadron, 6 rue Boussingault, 67083 Strasbourg Cedex, France*

Received 9 July 2001; in final form 8 January 2002

Abstract

Molecular motions in mono-hydrated racemic camphor sulphonic acid (±)-10-$C_{10}H_{16}O_4S^-$–H_3O^+ which is abbreviated as (CSA–H_2O) were investigated using incoherent neutron scattering techniques. Analysis of the intensity of the purely elastic scattering over a wide temperature range (4–340 K) carried out with a high-resolution backscattering spectrometer revealed the onset of molecular motions at ca. 100 K which could be observed on the 10^{-10} s time-scale up to $T = 180$ K. These motions were identified as 120° jumps of the methyl groups. Quasielastic measurements using both the backscattering and the time-of-flight techniques enabled to study this movement from 150 to 340 K. The corresponding characteristic time was found to follow an Arrhenius law with an activation energy $\Delta H = 12.0 \pm 0.2$ kJ mol^{-1}. All the methyl groups appear as dynamically equivalent. That result is at contrast with earlier studies on conducting polymers where CSA was introduced as a counter-ion and for which the intermolecular effects were found to strongly influence the dynamics. Inspection of the low frequency part of the vibrational spectrum evidences deformations of the C–C–S angle and rotational oscillations of the hydration molecules.

Keywords: Neutron scattering; Quasielastic scattering; Molecular dynamics; Methyl rotation; Camphor

1. Introduction

Numerous assemblies of camphor-based molecules in the solid state have been largely studied for many reasons and some of them usually form molecular solids exhibiting rich molecular dynamics. Among these, we brought a particular attention to camphor sulphonic acid, $C_{10}H_{16}SO_4$, hereafter denoted as CSA (Fig. 1(a)) because it has been used as a doping agent of polyaniline (PANI) in order to prepare highly conducting polymer films [1–4]. One of the most privileged techniques for the investigation of molecular dynamics in condensed phases is certainly inelastic scattering of slow neutrons which provides information about the geometry of the relevant motions and also

* Corresponding author. Fax: +33-476-51-4544.
E-mail address: ddjurado@spectro.ujf-grenoble.fr (D. Djurado).
[1] Also corresponding author.

0301-0104/02/$ - see front matter
PII: S0301-0104(02)00313-0

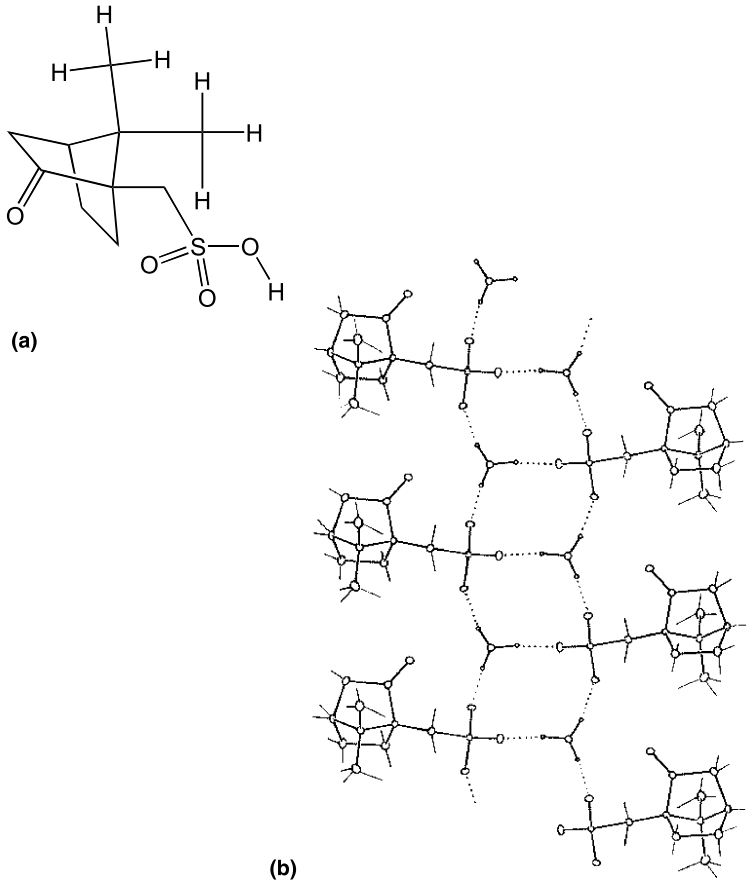

Fig. 1. (a) Chemical formula of camplor sulfonic acid, (b) crystallographic structure of 1(s)-(+)-10-camphor sulphonic acid monohydrate [10]. View along screw axis 2_1 parallel to ***b*** showing the hydrogen bonding arrangement. For clarity reasons, the hydrogen atoms on the camphor sulphonic ion are not represented: only their bonds with the carbon atoms are indicated by sticks. Small circles denote the hydrogen atoms involved in the hydrogen bonds with the water molecules.

about their characteristic times. Recently we performed by quasielastic neutron scattering a detailed analysis of the molecular dynamics of CSA inserted in between PANI chains [5–7]. We discovered an apparent relation between this dynamics and the electronic properties of the films. At this stage, it appeared crucial to characterise more precisely the molecular dynamics of CSA itself, taken in its stable hydrated phase. Specially, in order to better understand the interaction between the polymeric chain and CSA counter-ions it is necessary to differentiate any dynamical characteristics which would be intrinsic to the molecule from those arising from intermolecular effects. More precisely, in the study of the PANI/CSA system, the CSA methyl groups were found non-equivalent. To conclude definitely that these groups had their dynamics directly influenced by their local environment, for which they could constitute a microscopic probe we wanted to check whether that effect was not an intramolecular characteristic resulting from the chiral character of the CSA, as already observed with other molecules [8,9].

The time-scale range accessible to a given neutron spectrometer is usually restricted to one or two orders of magnitude. To get information over a wider energy range, it often required the same specimen to be investigated with several instruments having complementary characteristics. This

paper reports on several series of neutron quasielastic experiments by using three different spectrometers and performed with racemic (±)CSA hydrated solid phase containing one H_2O molecule per CSA. As far as we know the crystallographic structure of this compound has not been published, but the structure of the mono-hydrated enantiomeric form is well known [10] (Fig. 1(b)).

2. Neutron scattering theory

This section aims at giving a minimum of information about neutron scattering and especially about incoherent quasielastic neutron scattering (IQNS), referring to standard textbooks for a general survey of the neutron technique [11–14] or a description of quasielastic scattering [15,16]. We want to point out a few general characteristics to which we shall refer in the analysis of the data.

In a typical neutron scattering experiment monochromatic neutrons exchange both energy, $\hbar\omega$ and momentum $\hbar\boldsymbol{Q}$ during the scattering process. The latter is defined as $\boldsymbol{Q} = \boldsymbol{k} - \boldsymbol{k}_0$, where $\boldsymbol{k}$ and $\boldsymbol{k}_0$ are the scattered and incident wavevectors, respectively. As the incoherent scattering length of the hydrogen atoms ($b = 25.2 \times 10^{-15}$ m) is an order of magnitude larger than any other scattering length in the system, and as CSA contains a large fraction of hydrogen atoms, only hydrogen incoherent scattering is considered here.

The incoherent dynamic structure factor $\boldsymbol{S}(\boldsymbol{Q},\omega)$ is the time Fourier transform of the intermediate scattering function, $I(\boldsymbol{Q},t)$,

$$S(\boldsymbol{Q},\omega) = \frac{1}{2\pi}\int_{-\infty}^{+\infty} I(\boldsymbol{Q},t)\exp(-\mathrm{i}\omega t)\,\mathrm{d}t, \tag{1}$$

which itself is defined as

$$I(\boldsymbol{Q},t) = \sum_i b_i^2 \left\langle \mathrm{e}^{\mathrm{i}\boldsymbol{Q}\cdot\boldsymbol{R}_i(t)}\mathrm{e}^{-\mathrm{i}\boldsymbol{Q}\cdot\boldsymbol{R}_i(0)}\right\rangle. \tag{2}$$

The sum over i runs over the scattering nuclei in the sample and the thermal average denoted by the brackets holds for the vector positions of these nuclei, $\boldsymbol{R}_i(t)$ and $\boldsymbol{R}_i(0)$, at time t and at time 0, respectively. The hydrogen atoms of the system experience two types of molecular motions: rotations (reorientations of whole molecule or of chemical groups) and vibrations (phonons and internal vibrations).

The interpretation of the data is usually simplified by making the hypothesis that the different kinds of contributions to motions are essentially not coupled between them, because of their respective time-scales and amplitudes. Vibrational motions of a molecule occur on the 10^{-13}–10^{-14} s time-scale and may be considered as independent from diffusive-type rotations which are much slower (10^{-9}–10^{-12} s). That is mathematically expressed by writing the total scattering function as the convolution product of the respective scattering functions

$$S(\boldsymbol{Q},\omega) = S^{\mathrm{rot}}(\boldsymbol{Q},\omega) \otimes S^{\mathrm{vib}}(\boldsymbol{Q},\omega). \tag{3}$$

In the quasielastic region of the spectrum (which corresponds to energy transfers smaller than about 2 meV), the expression above takes the form

$$S(\boldsymbol{Q},\omega) = \mathrm{e}^{-\langle u^2\rangle \boldsymbol{Q}^2/3}\left[S^{\mathrm{rot}}(\boldsymbol{Q},\omega) + S^{\mathrm{inel}}(\boldsymbol{Q},\omega)\right]. \tag{4}$$

The Debye–Waller term $\exp[-\langle u^2\rangle \boldsymbol{Q}^2/3]$ is a scaling factor that describes the attenuation effect due to lattice phonons or molecule vibrational modes of lowest energy. $\langle u^2\rangle$ stands for the mean square amplitude of vibration. These motions also introduce the inelastic term $S^{\mathrm{inel}}(\boldsymbol{Q},\omega)$ which actually contributes only little to the total scattering in the quasielastic region in the form of a slowly varying function of energy which is most often taken into account as an energy-independent background

$$S^{\mathrm{inel}}(\boldsymbol{Q},\omega) = S^{\mathrm{inel}}(\boldsymbol{Q}). \tag{5}$$

Correlations between the positions of the same scatterer at initial time $\boldsymbol{R}(0)$ and at a later time $\boldsymbol{R}(t)$ diminish as a function of time and tend to disappear completely at infinite times. Consequently the thermal average occurring in the intermediate scattering function (2) can be evaluated by considering separately the initial and final positions of the scattering nucleus. Hence, from (2) and for a single scatterer

$$I(\boldsymbol{Q},\infty) = \left\langle \mathrm{e}^{\mathrm{i}\boldsymbol{Q}\cdot\boldsymbol{R}(\infty)}\right\rangle\left\langle \mathrm{e}^{-\mathrm{i}\boldsymbol{Q}\cdot\boldsymbol{R}(0)}\right\rangle. \tag{6}$$

The system being in thermal equilibrium, the distribution of the scattering nuclei is the same at both times, so that

$$I(\boldsymbol{Q},\infty)=\left|\left\langle e^{i\boldsymbol{Q}\cdot\boldsymbol{R}(\infty)}\right\rangle\right|^2=\left|\left\langle e^{-i\boldsymbol{Q}\cdot\boldsymbol{R}(0)}\right\rangle\right|^2. \quad (7)$$

In the case of a fully isotropic sample (liquid), at infinite times, the scattering nucleus can access any coordinate in space, independently of its initial position. Thus the average $I(\boldsymbol{Q},\infty)$ vanishes. Conversely in the case of whole molecule reorientations about centre of mass or of internal reorientations of chemical groups, the scatterers remain confined within a certain volume of space. Therefore at infinite times, the probability of finding the scatterer within the volume is equal to unity. $I(\boldsymbol{Q},\infty)$ is directly linked to the Fourier transform of the spatial distribution of the scattering centres [16] so it does not vanish and its variation with the momentum transfer, $\boldsymbol{Q}$, provides information about the size and the shape of the restrictive volume.

At any time, it is possible to separate formally $I(\boldsymbol{Q},t)$ into its time-independent part, $I(\boldsymbol{Q},\infty)$ and its time-dependent part $I(\boldsymbol{Q},t)-I(\boldsymbol{Q},\infty)$. The presence of a constant term gives rise by Fourier transform to a purely elastic component in the scattering function, hence

$$S^{\mathrm{rot}}(\boldsymbol{Q},\omega)=I(\boldsymbol{Q},\infty)\delta(\omega)+\frac{1}{2\pi}\int_{-\infty}^{\infty}[I(\boldsymbol{Q},t)-I(\boldsymbol{Q},\infty)]\times\exp(-i\omega t)\,dt. \quad (8)$$

In the most simple case $I(\boldsymbol{Q},t)$ decreases exponentially with time from its initial value $I(\boldsymbol{Q},0)$ with a single characteristic time, τ,

$$I(\boldsymbol{Q},t)=[I(\boldsymbol{Q},0)-I(\boldsymbol{Q},\infty)]\exp\left(-\frac{t}{\tau}\right)+I(\boldsymbol{Q},\infty), \quad (9)$$

and the expression of the scattering function involves a quasielastic component with a Lorentzian shape underlying a purely elastic component. Its half width at half maximum (hwhm) in energy unit is equal to $1/\tau$.

$$S^{\mathrm{rot}}(\boldsymbol{Q},\omega)=I(\boldsymbol{Q},\infty)\delta(\omega)+[I(\boldsymbol{Q},0)-I(\boldsymbol{Q},\infty)]\frac{1}{\pi}\frac{\tau}{1+(\omega\tau)^2}. \quad (10)$$

In the general case of more complicated reorientations or of several scattering atoms having different dynamics, as far as the movements remain diffusive in nature, the quasielastic component is expressed as a sum of several Lorentzian functions whose widths and relative contributions depend on the precise motions of individual atoms. In all cases the width of the quasielastic term is directly related to the characteristic times associated to the relevant motions of the scattering nuclei. The overall importance of the purely elastic component is directly linked to the Fourier transform of the spatial equilibrium distribution of the scattering centres. It has the dimension of a structure factor and is usually denoted as elastic incoherent structure factor (EISF). For instance the motion of a hydrogen atom of a methyl group is usually described as jumps on three energetically equivalent sites evenly distributed on a circle. The theoretical scattering law can be written (powder average) as [16]:

$$S^{\mathrm{rot}}(\boldsymbol{Q},\omega)=A_0(\boldsymbol{Q})\delta(\omega)+(1-A_0(\boldsymbol{Q}))\frac{1}{\pi}\frac{\Gamma}{\Gamma^2+\omega^2} \quad (11)$$

with

$$A_0(\boldsymbol{Q})=\frac{1}{3}(1+2j_0(\sqrt{3}\boldsymbol{Q}\cdot\boldsymbol{r})). \quad (12)$$

In expressions (11) and (12), $A_0(\boldsymbol{Q})$ is precisely the EISF, r is the distance of the hydrogen atom to the threefold symmetry axis, Γ is the jumping rate (which defines the hwhm of the quasielastic component) which is related to the methyl correlation time, τ_{meth}– mean residence time between two consecutive jumps – by $\Gamma=3/(2\tau_{\mathrm{meth}})$.

The energy resolution of any spectrometer is finite. Thus the elastic peak is never infinitely narrow but rather exhibits some shape characteristic of the instrument, generally triangular or Gaussian. The fwhm of this function determines the lower limit of the observable energy transfers accessible to the spectrometer. It corresponds to the slowest observable movements. Motions that occur on a too long time-scale give rise to very small energy transfers, which yield a quasielastic broadening too weak to be observed accurately. For instance typical energy width of the resolution of a backscattering spectrometer like IN10 (Institut Laue-Langevin (ILL), Grenoble, France, see

Section 3) is equal to about 1 μeV (fwhm). Assuming that a quasielastic broadening can be measured when its hwhm is at least 1/10 of this value, this instrument allows to investigate motions with a characteristic time faster than 6.6×10^{-9} s. The upper limit in energy accessible to a spectrometer determines the fastest motions which can be observed. The spectrometer abovementioned permits to investigate energy exchanges within the limits ±15 μeV. It corresponds to motions occurring on a time-scale of about 4.4×10^{-11} s. A faster dynamics of the scattering nuclei results in a wide broadening of the major part of which is located outside the instrument energy limits. Within the instrument energy window quasielastic scattering appears as a nearly flat background and the determination of its hwhm is very difficult. This point is particularly important in the interpretation of the data obtained by the so-called "fixed-window" technique. The time-of-flight spectrometer IN6 (ILL, Section 3) exhibits an energy resolution of the order of 80–150 μeV (fwhm). Its longest limit for dynamical phenomena is thus $2–4.4 \times 10^{-11}$ s. But it allows to observe quasielastic energy transfers up to about 2–4 meV (actually this limit is given by the discrimination between the quasielastic region and inelastic vibrational part of the spectra). Thus dynamical processes with short characteristic times ($3.3–1.6 \times 10^{-13}$ s) can be investigated. With IN6, by considering the edge of the experimental energy spectrum, it is possible to obtain the purely inelastic spectrum for low energy vibrational modes ($1 < E < 50$ meV). In fact, the quantity directly visualised in these experiments corresponds to the function directly deduced from the inelastic law as:

$$p(\bar{\alpha}) = \beta\hbar\omega[\exp(-\beta\hbar\omega) - 1]\frac{S^{\text{inel}}(\boldsymbol{Q},\omega)}{\bar{\alpha}} \tag{13}$$

with $\bar{\alpha} = (\hbar^2\boldsymbol{Q}^2)/(2mk_BT)$ where the usual quantity $\beta = 1/(k_BT)$ has been introduced. By simple extrapolation (13) provides a determination of the vibrational frequencies distribution $G(\omega)$.

$$\lim_{\boldsymbol{Q}^2\to 0} p(\bar{\alpha}) = G(\omega). \tag{14}$$

The analysis of the dynamical behaviour of a system over a wide temperature range generally requires using several spectrometers having different characteristics each of them being adapted to a particular interval of temperature. But when passing from an instrument to another and increasing the temperature, great care has to be taken to check whether it is actually the same motion which is investigated or if a new kind of movement has appeared.

3. Experimental

The IQNS experiments were performed at the high-flux reactor of the ILL (Grenoble, France). In a first series of experiments, the dynamics of CSA was investigated with the time-focusing time-of-flight spectrometer IN6 [17], operating with an incident wavelength $\lambda = 5.12$ Å. 89 spectra were recorded simultaneously for different scattering angles ranging from 14.7° to 113.5°. CSA powder was held in a flat circular aluminium container, 50 mm diameter and 0.3 mm thickness. Two series of experiments were carried out, with two instrument energy resolutions obtained by setting the sample at $\alpha = 45°$ or $\alpha = 135°$ with respect to the incident beam. The disadvantage of the former configuration is the shielding of the detectors over an angular range of about 15° on each side of the sample plane. But an energy resolution of typically 80 μeV, fwhm can be kept nearly constant over the whole scattering vector angle ($0.31\ \text{Å}^{-1} < \boldsymbol{Q} < 2.05\ \text{Å}^{-1}$). Conversely, in the transmission geometry ($\alpha = 135°$) the resolution varies from 77 μeV at small scattering angle to about 120 μeV for the largest values. For each geometry the actual energy resolution was measured with a vanadium plate, 1 mm in thickness, which also served for calibration of the detector efficiencies.

The obtained time-of-flight spectra were corrected for absorption and scattering from the container. They were transformed into energy spectra using the program INX of the ILL library. Detectors clearly contaminated with Bragg elastic scattering were discarded. The other spectra were grouped into a series of 15 spectra. Experiments were performed at temperatures ranging from 270 to 320 K. The temperature stability was about 1 K.

Another series of experiments was performed with the high-resolution backscattering spectrometer IN10 [17] with a wavelength of 6.28 Å, an energy resolution of 0.9 μeV (fwhm) and an energy window of about ±15 μeV. Here the investigated time-scale was 10^{-9}–10^{-10} s, thus CSA was studied in a temperature range from 150 to 180 K. The sample was held in a slab aluminium container with rectangular shape (26×40 mm^2) and 0.5 mm thickness. The transmission was about 0.95. The specimen was set perpendicular to the beam ($\alpha = 90°$) and seven spectra were recorded at average scattering angles between 29° and 156°. Great care was taken to avoid contamination of the recorded intensity by coherent elastic scattering and the analyser angles corresponding to Bragg reflections were shielded with cadmium. The accessible momentum transfer range was similar to IN6 with $\boldsymbol{Q}$ ranging from 0.5 to 1.96 Å^{-1}. The detector efficiencies were calibrated from the measurement of a vanadium standard with 2 mm in thickness. The energy resolution was determined from the scattering of the sample itself at $T = 4$ K. At this temperature, all motions responsible for quasielastic scattering have disappeared and the scattering is purely elastic. Quasielastic measurements were performed at 150, 162 and 180 K. Moreover, during the temperature changes for the analysis at 4 K the Doppler machine was turned off, so that only the neutrons scattered without energy change were detected. In these "fixed-window" measurements data were collected and binned every five minutes, while the temperature was continuously modified from 340 to 4 K. Data were reduced using the program SQW of the ILL library.

CSA was also analysed at intermediate energy resolution (fwhm 8 μeV) with the thermal backscattering spectrometer IN13 [17], with a 2.23 Å wavelength. The energy window was 100 μeV, and the accessible time-scale 10^{-10}–10^{-11} s. The sample was analysed in a transmission geometry ($\alpha = 135°$). Data were recorded at 28 scattering angles, ranging from 5.84 ($\boldsymbol{Q} = 0.29$ Å^{-1}) to 128.18° ($\boldsymbol{Q} = 5.03$ Å^{-1}). After inspection and elimination of the spectra contaminated with Bragg scattering, they were grouped into a series of 16 spectra corresponding to average values ranging between $2\theta = 32.8°$ and $2\theta = 122°$ (1.6 Å^{-1} $< \boldsymbol{Q} <$ 4.9 Å^{-1}). Sample and container were the same as for IN10 experiments. Measurement of a vanadium standard (2 mm in thickness) was used for calibration of the detectors. CSA was placed in a cryofurnace and investigated at three temperatures ($T = 200$, 225 and 250 K, namely) intermediate between the temperature ranges covered with IN10 and IN6.

We measured a typical transmission rate of 92% for the sample and evaluated that the multiple scattering effect was less than 5% of the total scattering.

4. Data analysis

4.1. Fixed-window measurements

With backscattering spectrometers, the fixed-window method is commonly used. In this technique the neutrons incoming on the sample have exactly the energy that is selected by the analysers. So only the neutrons scattered without energy change (within the instrument resolution) are recorded. In the same time an external parameter (generally the sample temperature) is varied. The occurrence of a molecular motion on the resolution time-scale results in the onset of quasielastic broadening and thus in a reduction of the detected elastic intensity [18]. This technique allows the evolution of the dynamics to be inspected within a very large temperature range. Clearly these observations must be carried out in combination with quasielastic measurements in order to get a full description of the dynamics of the system.

In Fig. 2 the evolution of the elastic intensity for CSA as recorded on IN10 has been reported as a function of temperature for several values of the scattering angle 2θ. Three regions are clearly visible.

(i) In the low temperature range ($T < 100$ K) all the diffusive molecular motions are too slow to give rise to any quasielastic broadening of the scattering function while the inelastic contribution is so small it can be neglected. Accordingly, the recorded intensity can be considered as purely elastic. Thus, its evolution with temperature is only

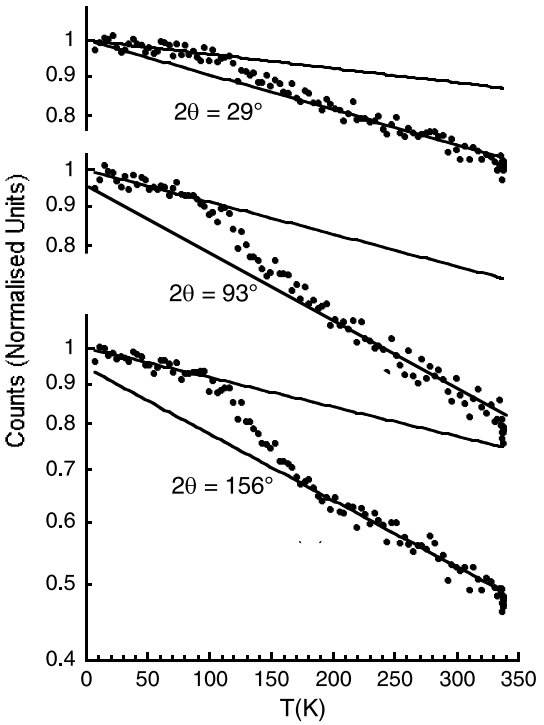

Fig. 2. Temperature evolution of the purely elastic intensity for several $\boldsymbol{Q}$-values obtained from elastic scan with the IN10 spectrometer. The straight lines represent the theoretical decrease predicted by a single Debye–Waller term. (They were refined to experimental data at $T < 100$ K and $T > 170$ K, respectively.) The intensities for the different detectors were normalised to each other at $T = 0$ K.

governed by the Debye–Waller term in Eq. (4), according to

$$S(\boldsymbol{Q}, \omega = 0) = C^{\mathrm{ste}} \mathrm{e}^{-\boldsymbol{Q}^2 \langle u^2 \rangle / 3}. \tag{15}$$

At each temperature, the $\boldsymbol{Q}$-dependence permits to extract a mean square displacement $\langle u^2(T) \rangle$ that describes purely harmonic vibrations. It depends linearly on the temperature as it can be clearly observed in Fig. 2 for $T < 100$ K.

(ii) At higher temperature (100 K $< T <$ 170 K) the elastic intensity is decreasing more rapidly. That means in this temperature range, the scattering function broadens due to the occurrence of a quasielastic component now visible with the resolution of the spectrometer. This behaviour is directly governed by physical parameters of the now visible diffusive component of motions such as the activation energy, the attempt frequency, the geometry of the volume accessible to proton, etc. Now, still considering (15), it is possible to extract an "effective" mean square displacement that takes into account both vibrational and diffusive motions and which is a rough characteristic of the amplitude of the movements. It should be noted that such procedure is widely used for dynamical study of biological macromolecules [19].

(iii) For $T > 170$ K (Fig. 2) the broadening becomes too large to be still accurately measured. Now the major part of the quasielastic scattering is outside the instrument window and the total recorded intensity becomes less and less sensitive to the increase of broadening with temperature that results in quasi-constant additional intensity added to the flat background of the signal. Accordingly, data reported in Fig. 2 follow again the evolution governed by the Debye–Waller prefactor as it is written in Eq. (15). It should be noted that the slopes in Fig. 2 are not identical on both sides of the step decrease. This is due to both the exact evolution of the quasielastic component with the temperature and to the more complex nature of $\langle u^2 \rangle$ compared to the low temperature range. This analysis is fully detailed in [18,20].

In Fig. 2, for each scattering angle, two straight lines are indicated. They were obtained from least-square refinements of the plotted values in the temperature ranges $T < 100$ K and $T > 170$ K. The value predicted by the line at $T = 0$ in the low-temperature regime was used to normalise together the data for different angles. Both lines do not cross together exactly at $T = 0$. This is due to the more or less arbitrary way with which the high temperature domain for the least square refinement procedure has been delimited.

If, we consider again the temperature range which contains the step decrease of intensity ($100 < T < 170$ K), we can try now to estimate the EISF by evaluating more precisely the constant term of Eq. (15):

$$\begin{aligned} S(\boldsymbol{Q}, \omega = 0) &= C^{\mathrm{ste}} \mathrm{e}^{-\mathrm{Q}^2 \langle u^2 \rangle / 3} \\ &= \mathrm{e}^{-\boldsymbol{Q}^2 \langle u^2 \rangle / 3} [A_0(\boldsymbol{Q}) + S^{\mathrm{inel}}] \\ &\approx \mathrm{e}^{-\boldsymbol{Q}^2 \langle u^2 \rangle / 3} [A_0(\boldsymbol{Q})]. \end{aligned} \tag{16}$$

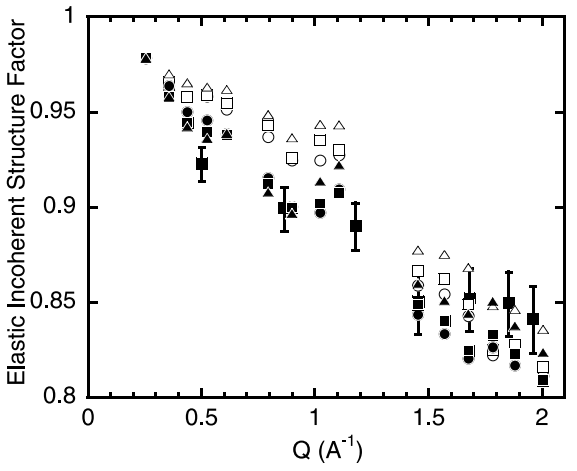

Fig. 3. EISF determined from analysis of the decrease of the purely elastic intensity measured by an elastic scan on the instrument IN10 (Fig. 2) (full squares with error bars). Error bars were evaluated from the deviations of the parameters of the straight lines refined on each side of the step decrease ($T < 102$ K and $T > 166$ K, respectively). EISF values obtained with IN6 by separation of the spectra into their elastic and quasielastic parts are also reported; triangles: $T = 270$ K, squares: $T = 300$ K, circles: $T = 330$ K; full symbols: transmission geometry, open symbols: reflection geometry.

The values we found are reported in Fig. 3 for the $\boldsymbol{Q}$-values accessible with IN10. They were obtained from the difference of the intensities predicted by the two straight lines at the temperature corresponding to the end of the step decrease ($T = 166$ K namely), where the quasielastic scattering is much broader than the instrument resolution. Several calculations were carried out using the different estimations of the straight lines obtained on each side of the step decrease by varying the refinement parameters. They yielded an estimation of the error bars reported in Fig. 3. Whilst it is not very accurate this method provides an estimation of the EISF of the relevant motion. Actually the decrease observed on the IN10 $\boldsymbol{Q}$-range is not very important (from 1 to 0.85). It seems that some minimum value was reached for $1.5\ \text{Å}^{-1} < \boldsymbol{Q} < 2.0\ \text{Å}^{-1}$ but no definite conclusion can be drawn about the exact nature of the observed motions.

However, it is important to point out that a single step decrease is visible in Fig. 2 over the full temperature range 10–330 K. The spectrometer IN10 probes the microscopic motions on the 10^{-10} s time-scale, i.e. on a slower time-scale than the two other instruments IN13 and IN6. Therefore the motion which appears on that instrument between 100 and 150 K should be observed at higher temperatures with the thermal backscattering and the time-of-flight spectrometers. At this stage it is now necessary to inspect carefully the EISF recorded on the two other spectrometers in order to check in which extent this motion detected on IN10 is recovered on IN13 and IN6, if it is the only one and which kind of motion it is.

4.2. Inspection of the elastic incoherent structure factor

The EISF is more classically deduced from an analysis of incoherent quasielastic data. It is defined as the long-time limit of the intermediate scattering function $I(\boldsymbol{Q}, t)$ and in principle, it could be obtained by a simple Fourier-transformation of the scattering law $S(\boldsymbol{Q}, \omega)$. But actually several conditions rend this procedure rather imprecise. The EISF is most commonly obtained from a separation for each experimental spectrum of the scattered intensity into its purely elastic $I_{\text{elas}}(\boldsymbol{Q})$ and its quasielastic $I_{\text{quasi}}(\boldsymbol{Q})$ parts and the subsequent evaluation of the ratio

$$\text{EISF}(\boldsymbol{Q}) = \frac{I_{\text{elas}}(\boldsymbol{Q})}{I_{\text{elas}}(\boldsymbol{Q}) + I_{\text{quasi}}(\boldsymbol{Q})}. \tag{17}$$

The EISF is equal to unity at $\boldsymbol{Q} = 0$. Then it decreases as a function of $\boldsymbol{Q}$ and generally exhibits a minimum in a $\boldsymbol{Q}$-range such that $\boldsymbol{Q} \cdot \boldsymbol{R} \approx \pi$, where R is a characteristic length in real space of the order of the dimensions of the relevant motions (i.e. the movements observed on the instrument time-scale). Thus direct information can be obtained about the trajectories of the protons, provided that the EISF can be extracted over a $\boldsymbol{Q}$-range in relation with the lengths of the displacement under interest. Actually, if $\boldsymbol{Q} \cdot \boldsymbol{R} < \pi$ the distinction between several hypotheses for the molecular dynamics may be ambiguous, especially if a large fraction of the protons are immobile and give rise to a large amount of purely elastic scattering.

IN13 has a unique characteristic to combine a very large accessible $\boldsymbol{Q}$-range ($\boldsymbol{Q} < 5.5\ \text{Å}^{-1}$ with

an intermediate energy resolution (8 μeV, fwhm). Therefore to get some insight about the relevant dynamics we were concerned with CSA, the IN13 data were first inspected. One can note first that it has been possible to extract an experimental value of the EISF on spectra recorded in the 200–250 K temperature range i.e. a little bit displaced towards higher temperatures compared to that found with IN10. A very simple approach was chosen to separate the experimental spectra into their purely elastic and quasielastic contributions. The broadened part of each spectrum was described by a unique Lorentzian function, analytically folded with the instrument resolution. The latter was chosen to be gaussian, and its parameters were determined from refinement of the measurements of the CSA sample at $T = 20$ K, where all diffusive motions have disappeared. Conversely, the purely elastic intensity in each spectrum was reproduced by the experimental data. A weight parameter controlled the respective amount of the two contributions.

Good fits were obtained for all the refined spectra, for each temperature of experiment, confirming that in all cases the quasielastic broadening could effectively be described by a single Lorentzian function. Another important point is the agreement between the EISF values extracted at different temperatures (Fig. 4). Because of the rather poor neutron flux of the instrument, the uncertainties on the determined values are important.

There is nevertheless a clear indication that the same geometry of the motions is observed over the whole temperature range. The same procedure was applied to IN6 spectra measured at $T > 270$ K. The extracted values are reported in Fig. 3 and fully agree with the IN10 results at lower temperature ($T = 166$ K). The results thus obtained on IN13 and IN6 confirm that the same motion is indeed observed with both spectrometers, on the different time-scales corresponding to their respective energy resolutions.

4.3. Variation of the quasielastic width with momentum transfer

Another information that can be easily extracted from the data is the variation of the overall

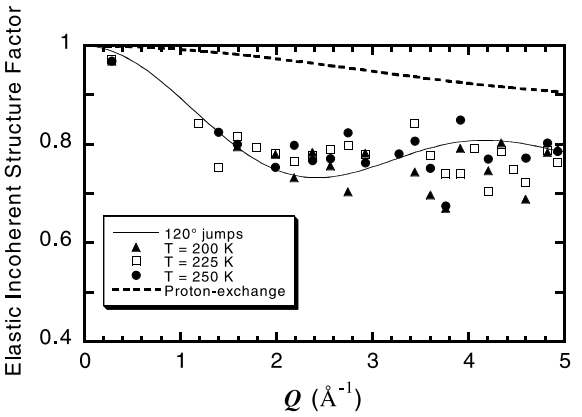

Fig. 4. EISF determined from the separation of the IN13 spectra into their purely elastic and quasielastic parts ($T = 200$, 225 and 250 K). The full curve is the theoretical variation predicted by a model allowing for 120° jumps of the CSA methyl jumps. The model based on a proton exchange along the hydrogen bond is also indicated (dashed line).

width of the quasielastic part of the scattered intensity as a function of the momentum transfer. To our opinion this analysis is too often neglected although it can be very useful to discriminate among several plausible dynamical models. Theoretical models usually employed to mimic the dynamic of a microscopic system generally lead to scattering laws where the quasielastic part is expanded in a series of Lorentzian functions. Their respective hwhm depends explicitly on few characteristic times associated to the details of the molecular motions. The relative contributions of these Lorentzian functions change with $\boldsymbol{Q}$, according to the variations of their related quasielastic structure factors. Therefore the overall hwhm of the broadened part of the spectra is $\boldsymbol{Q}$-dependent. However, in some cases the broadening remains constant over the whole $\boldsymbol{Q}$-range. The most common situations are the two-site and the three-site jump models. Respective examples are the proton exchange mechanism between two equivalent (or not) sites and 120° reorientations of methyl groups about their three-fold symmetry axis [16]. In the system under study, both models are possible. The two-site jump can occur along one hydrogen bonding connecting one CSA molecule to one water molecule and the tree site jump

can concern of course the methyl rotation. It should be noted that the proportion of mobile hydrogen atoms, respectively, involved in these two processes is 1:3 and accordingly the quantitative differentiation in between the two models should be possible. Finally, because the $\boldsymbol{Q}$-dependence of the hwhm is directly related to the relative importance of the structure factors, distinction between various models is often possible at large $\boldsymbol{Q}$-values, like in the case of the EISF.

As it can be seen in Fig. 5, in all cases, the hwhm of the quasielastic part of corresponding spectra is clearly independent of the momentum transfer. Strongest deviations appear for the two highest temperatures that were analysed with a lower statistics. Especially at large scattering angles ($\boldsymbol{Q}^2 \approx 16$–$25$ Å^{-2}) the attenuation of the signal from the Debye–Waller term becomes

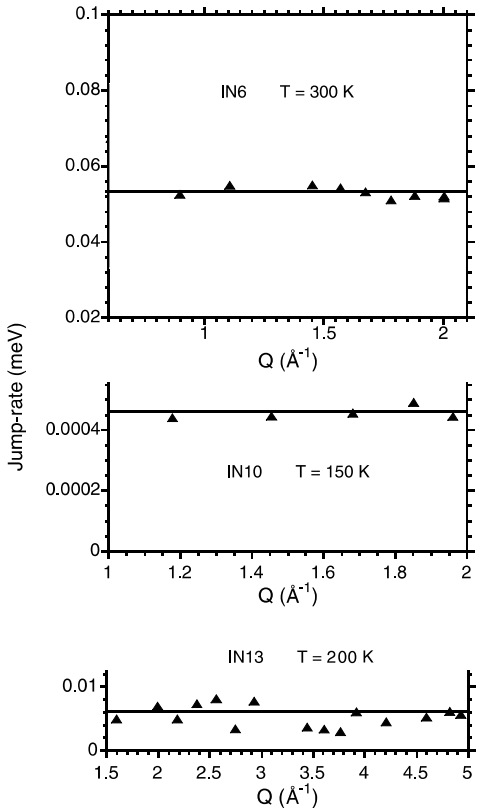

Fig. 5. Halfwidth at half maximum of the quasielastic part of the spectra obtained with the different instruments.

important and the distinction between quasielastic intensity (i.e. scattering associated to diffusive motions) and inelastic background (i.e. scattering due to vibrational modes) is more difficult. Moreover, as it is shown in the Fig. 4, all the experimental values are in very good agreement with the predictions of the model assuming only 120° reorientations of methyl groups. Clearly the model based on a proton exchange mechanism along the hydrogen bond can be ruled out.

4.4. Refinement of the jump model

Spectra recorded at the same temperature with the same instrument were refined simultaneously, on the basis of the model of 120° jumps of methyl groups alone. Good fits were obtained at all temperatures. Typical results are illustrated in Fig. 6. Because of the rather small relative amount of quasielastic scattering, spectra are presented on a logarithmic scale. That representation better evidences the agreement between theoretical and experimental values, whatever the magnitude of the signal both for the elastic peak and in the wings of the spectra. Especially, the relative amount of elastic scattering of all the spectra could be fairly reproduced. Similarly the quasielastic broadening observed at the various scattering angles was satisfactorily described by a unique value at each temperature.

The values of the correlation times associated with methyl reorientations are plotted in Fig. 7 as a function of the reciprocal of the temperature. A straight line can be drawn across the experimental points. It corresponds to the following Arrhenius law:

$$\tau(s) = 1.0 \times 10^{-3} \exp(\Delta H/RT) \qquad (18)$$

with an activation energy $\Delta H = 12.0 \pm 0.2$ kJ mol^{-1}.

4.5. Inelastic part of IN6 spectra

The inelastic parts of the spectra obtained with IN6 are reported in Fig. 8. They were obtained in energy gain for neutrons, so a strong increase of the intensity as a function of the temperature is observed. Spectra were not corrected for

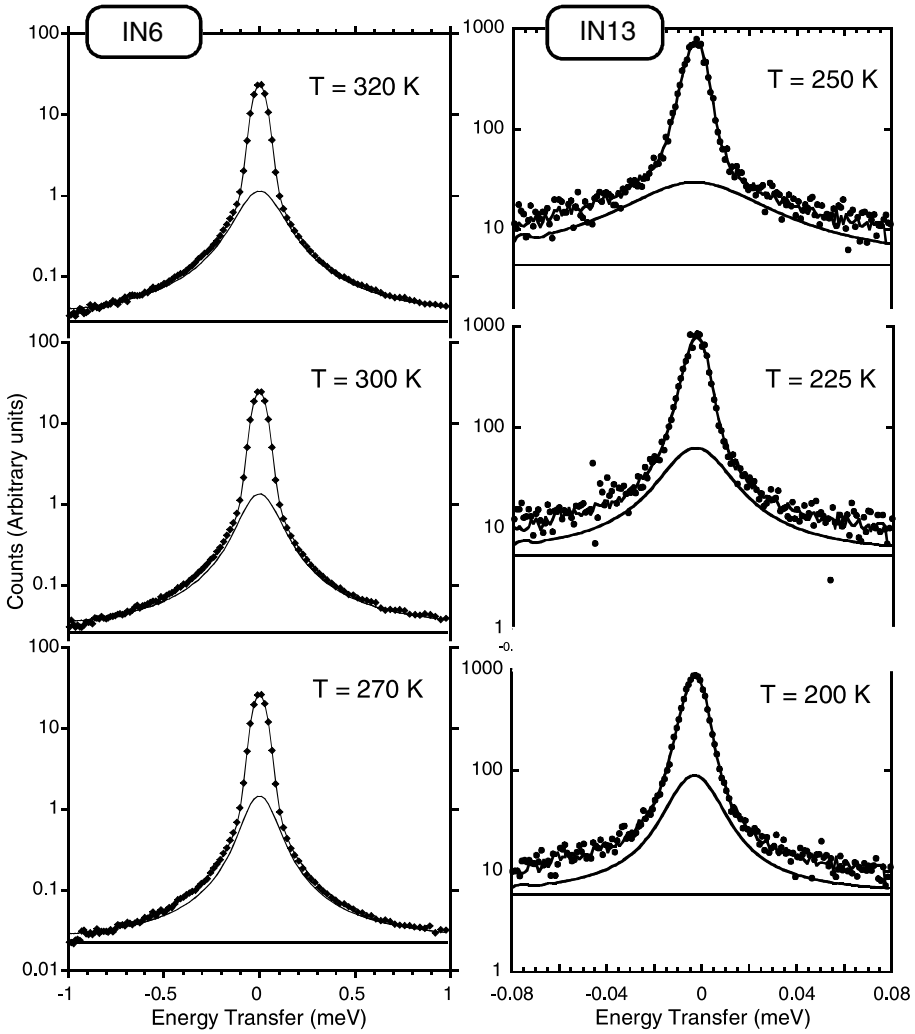

Fig. 6. Typical examples of refinements for quasielastic spectra measured with IN13 and IN6. The separation between purely elastic, quasielastic and inelastic (vibrational) contribution is indicated.

multiphonon effects that are particularly important at the largest energy transfer values. But the spectrometer energy resolution rapidly broadens in the inelastic region and this contribution becomes featureless. No variation of the peak positions is observed, neither with temperature nor with momentum transfer. On the other hand the peaks clearly visible between 10 and 40 meV are characteristic of internal vibrations. Recently a calculation of the vibrational modes in this compound was started. A full agreement is still not obtained. Nevertheless this study shows that methyl torsions are involved in the bands between 10 and 40 meV. For instance the peaks at 11 and 21 meV mainly correspond, respectively, to in-phase and out-of-phase torsions of the two CH_3 groups of a CSA molecule. The other bands at 15 and 19 meV involve a rotation of a unique methyl group coupled with a deformation of the molecular cage and a rotational oscillation of the water molecules. In the region of 25 meV the calculations reveal a wagging of the CH_3 with simultaneously a motion of the hydrogen atoms of the CH_2 group bonded to the sulphur atom perpendicular to the HCH plane.

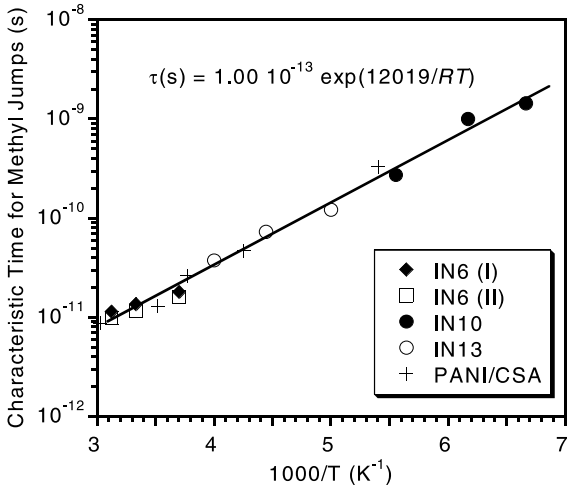

Fig. 7. Arrhenius plot of the characteristic time for 120° jumps of the methyl groups of the CSA molecules as obtained with the three spectrometers. Two sets of values are reported for IN6, corresponding to different sample orientations: (I) transmission geometry, (II) reflection geometry. Most probable values of the centre of the distribution of correlation times in the case of PANI/CSA compound [7] are also reported.

Neutron spectroscopy is sensitive to the amplitude of the hydrogen displacements. It is worth to point out that the relative importance of the mode at 25 meV tends to increase with temperature. In the same time its broadening also increases, an indication of a possible damping. That observation is close to the occurrence in conducting PANI [6,7] of a motion of the whole CSA counter-ion about its equilibrium position, with diffusive nature which gives rise to quasielastic broadening of the high resolution spectra at high temperature.

The bands observed below ca. 10 meV originates essentially from external modes of the CSA molecule i.e. lattice modes recovering motions of molecular species having big masses compared to a methyl group for example. However, it should be noticed that calculations also predict a mode of deformation of the CCS angle (see Fig. 1(a) and (b)) in this low energy domain (<10 meV).

5. Summary and discussion

The technique of incoherent neutron scattering has proved to be very powerful by allowing us to obtain clear information about the dynamics of the CSA molecule in its hydrated crystalline state. Several spectrometers with different characteristics giving access to complementary energy and momentum transfer ranges were used to cover a wide temperature interval. Fixed-window measurements carried out with the high-resolution spectrometer IN10 revealed the onset of a single molecular motion. The latter gives rise to a quasielastic broadening which, on the 10^{-10} s timescale appears above $T = 100$ K and can be observed up to T = 180 K. The characteristic ability of the thermal backscattering spectrometer IN13

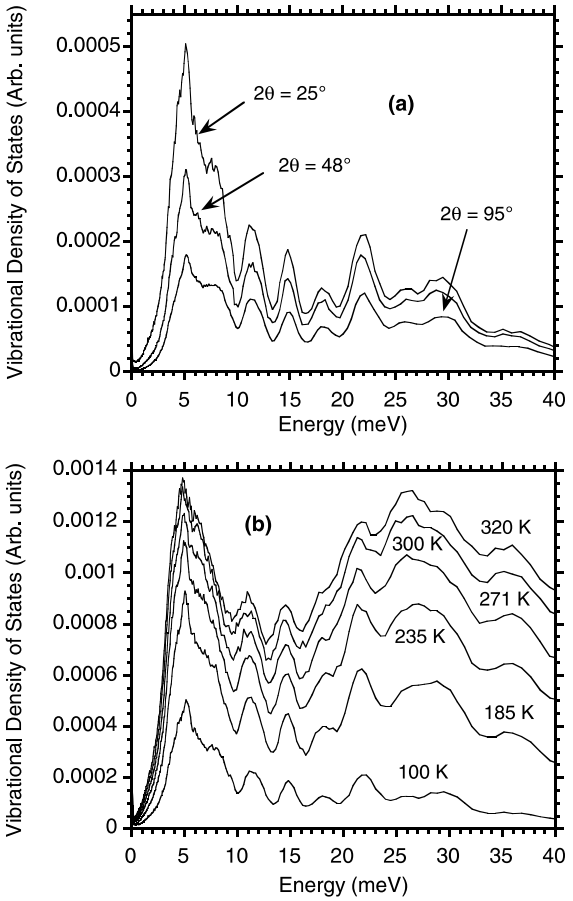

Fig. 8. Inelastic scattering for CSA: (a) data measured at $T = 100$ K have been grouped into three spectra corresponding to average scattering angles 25°, 48° and 95° (from top to bottom); (b) evolution with temperature of the same spectrum corresponding to a scattering angle of 25° ($T = 100$, 185, 235, 271, 300 and 320 K, from bottom to top).

to provide quasielastic spectra over a very large $\boldsymbol{Q}$-range, while keeping an intermediate energy resolution permitted to identify unambiguously this motion. The experimental EISF extracted from the quasielastic data was found to correspond to 120° jumps of the CSA methyl groups, all the other atoms being kept fixed. Especially the possibility of a proton exchange mechanism along the hydrogen bonds between water and CSA molecule could be unambiguously discarded. This conclusion was confirmed by the inspection of the hwhm of the broadened part of the spectra, which was found constant over the whole $\boldsymbol{Q}$-range. EISF values were also extracted from the quasielastic data obtained with IN10 and IN6, and, with less accuracy from IN10 fixed window measurements. All of them are in accordance with IN13 values but because of their restricted $\boldsymbol{Q}$-range ($\boldsymbol{Q} < 2$ Å^{-1}) they do not permit a definite conclusion about the nature of the observed motion, so far as they are considered alone. It is of major importance that similar EISF values were found, whatever the sample temperature. This result confirms that from 100 to 340 K we are concerned with the same geometry for the hydrogen displacements and is in agreement with the observation of a single step decrease in the evolution of the purely elastic intensity.

By combining data obtained with the three spectrometers it was possible to derive an Arrhenius law for the relevant characteristic time, with an activation energy $\Delta H = 12.0$ kJ mol^{-1}. Especially, all methyl groups could be considered as dynamically equivalent. That result is at variance with the conclusions of the study of conducting PANI protonated by CSA and it confirms that inspection of methyl group dynamics can probe their local environment. When the CSA molecules are inserted in between PANI polymer chains, methyl jumps were also observed but at each temperature the correlation time was found distributed around an average value [6,7]. Actually, only at high temperature ($T > 300$ K) the methyl groups could be considered as equivalent, each of them exploring a similar energetic environment. This regime disappeared when the temperature was lowered and the differences of molecular environments were progressively revealed. A very striking result is the Arrhenius plot of the average value which is very similar to the case of pure hydrated CSA, with an activation energy equal to 12.5 kJ mol^{-1} [6,7] and Fig. 7. That is a clear indication that the major part of the potential occurs from intramolecular interactions. As for the weaker intermolecular contribution, it manifests itself especially in the case of the disordered state. In that case it differs when passing from one CSA ion to another and varies with temperature, thus leading to a distribution of correlation times. As for the CSA in the ordered regions of the polymeric compound, their behaviour is close to the dynamics of crystalline CSA, and the characteristic time associated to reorientations of their methyl groups follows an Arrhenius law.

At high temperature ($T > 300$ K) the CSA counter-ions in PANI were found to also undergo a rigid body motion giving rise to a clear broadening in backscattering quasielastic experiments. That is at variance with the present case where no extra decrease of the elastic intensity appeared with the fixed-window measurements. Whole molecule diffusive motions are certainly much more hindered in crystalline CSA than in PANI compound. Fig. 1(b) shows that any CSA molecule is linked by three hydrogen bonds with three water molecules. The network of hydrogen bonds gives the crystallographic structure a rigid character so that large-amplitude oscillations about the bond with the water molecule are unlikely to occur. Nevertheless analysis of the vibrational part of the spectra reveals a strong coupling between methyl torsions and camphor cage distortions. Moreover a deformation of the CCS angle and a rotational excitation of the water molecules were also observed. It is not ruled out that similar couplings also occur in conducting PANI. One can imagine that in the PANI compound the CSA ion is not so tightly bonded to the polymer chain as it is linked to the water molecules in the present hydrated crystalline phase. Consequently the CCS angle deformation is over-damped and leads to the observed quasielastic scattering in PANI–CSA. That is perhaps a first lead in the understanding of the link between the electronic properties and the CSA counter-ion motions, which was clearly pointed out.

Acknowledgements

We are thankful to B. Suchod (LSP) for giving us detailed information on crystallographic characteristics of (1s)-(+)-10-camphor sulphonic acid monohydrate. We are also grateful to M. Johnson (ILL) for communicating his first results of calculations of vibrational spectra.

References

[1] Y. Cao, P. Smith, A.J. Heeger, Synth. Metals 48 (1992) 91.
[2] Y. Cao, A.J. Heeger, Synth. Metals 52 (1992) 193.
[3] M. Reghu, Y. Cao, D. Moses, A.J. Heeger, Phys. Rev. B 47 (1993) 1758.
[4] D. Djurado, Y.F. Nicolau, P. Rannou, W. Luzny, E.J. Samuelsen, P. Terech, M. Bée, J.L. Sauvajol, Synth. Metals 101 (1999) 764.
[5] M. Bée, D. Djurado, J. Combet, M. Telling, P. Rannou, A. Pron, J.P. Travers, Physica. B 301 (2001) 49.
[6] D. Djurado, J. Combet, M. Bée, P. Rannou, A. Pron, Synth. Metals 119 (2001) 411.
[7] D. Djurado, J. Combet, M. Bée, P. Rannou, A. Pron, J.P. Travers, Phys. Rev. B, submitted.
[8] N.D. Morelon, M. Bée, J. Combet, Chem. Phys. 261 (2000) 75.
[9] G.R. Kneller, K. Doster, M. Settles, S. Cusack, J.C. Smith, J. Chem. Phys. 97 (12) (1992) 8864.
[10] K. Fuji, M. Node, S. Terada, M. Murata, H. Nagasawa, T. Taga, K. Machida, J. Am. Chem. Soc. 107 (1985) 6404.
[11] P.A. Egelstaff, Thermal Neutron Scattering, Academic Press, New York, 1971.
[12] S.W. Lovesey, Theory of Neutron Scattering from Condensed Matter, Clarendon Press, Oxford, 1984.
[13] G.L. Squires, Introduction to the Theory of Thermal Neutron Scattering, Cambridge University Press, Cambridge, 1978.
[14] G. Kostorz, Neutron Scattering in Material Science, Academic Press, New York, 1978.
[15] T. Springer, Quasielastic Neutron Scattering for the Investigation of Diffusive Motions in Solids and Liquids; Springer Tracts in Modern Physics, Springer, Berlin, 1972.
[16] M. Bée, Quasielastic Neutron Scattering: Principles and Applications in Solid State Chemistry, Biology and Materials Science, Adam & Hilger, Bristol, 1988.
[17] See all information on http://www.ill.fr.
[18] B. Frick, L.J. Fetters, Macromolecules 27 (1994) 974.
[19] G. Zaccaï, Science 288 (2000) 1604.
[20] B. Frick, A. Magerl, Y. Blanc, R. Rebesco, Physica B 234–236 (1990) 1177.